

Supporting Information

Layer-dependent photocatalytic oxidation in two-dimensional Tellurene for integrated photonic resonance trimming

Dun Mao^{1*}, Yixiu Wang^{1,2,3}, Hwaseob Lee¹, Lorry Chang¹, Feifan Wang¹, Darren Wu¹, Yahui Xiao¹, Boshu Sun¹, Kaleem Ullah¹, Karl Booksh⁴, Wenzhuo Wu², Tingyi Gu^{1*}

I. Comparison to other resonance trimming schemes in silicon micro-resonators**Table S1.** Comparison of resonant wavelength tuning schemes in silicon micro-resonators

Mechanism	Additional source?	Laser wavelength	Fluence	Hybrid WG Δn_{eff}	Quality factor change
Silicon photo-oxidation [27-28]	Top exposure	532 nm	120J (cw)	~0.01 (derived)	Small (-62% [28], 54% [27])
Hybrid 2D Te photo-oxidation (this work)	No	1550 nm	2.55 mJ (cw)	0.062 ^{b)}	No
Hybrid GST PT ^{a)} [S1-S2]	No	1550 nm	Sub-nJ (pulsed)	0.06 +0.03i ^{b)}	Large contrast
Hybrid GSST PT [S3]	Top exposure	633 nm +780 nm	13-400 nJ (pulsed)	0.04 +0.007i ^{b)}	Small
Hybrid vdW In ₂ Se ₃ PT [S4]	Top exposure	1064 nm	0.25 nJ (pulsed)	0.03 ^{b)}	Small
Silicon strain ^{c)} [S5]	Strain/stress	--	--	10 ⁻⁴	Small
Thermal tuning ^{c)}	Integrated heater	--	--	10 ⁻²	No
Carrier injection ^{c)} [S6]	Integrated p/n junction	--	--	10 ⁻⁴	↓(absorption)

^{a)}PT: Phase transition; ^{b)}: The effective index change of the hybrid waveguide is estimated based on 10 nm thick film for Te, GST, GSST, and 50 nm layered In₂Se₃. ^{c)}Grids filled with grey: approaches used in monolithic silicon photonics but requires sustaining excitation power and additional substrate cooling

II. House-made setup for 1064nm laser top exposure and in-situ morphology monitoring

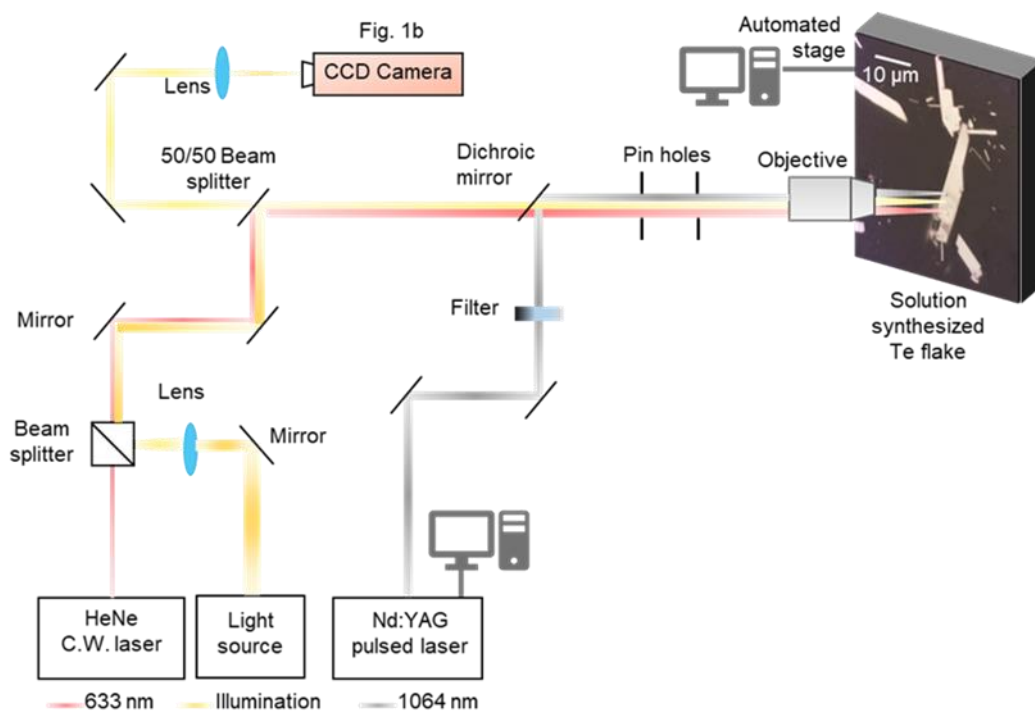


Figure S1. Optical setup for 1064 nm laser processing of solution synthesized 2D Te flakes. Schematics of direct laser writing setup. Three light sources are coupled onto the chip for alignment (633 nm cw laser), illumination (Tungsten bulb), and laser writing (1064 nm, ~ 1ns pulse duration, and 600 kHz repetition rate). The sample is mounted on a piezo-controlled xyz linear translation stage.^[S7]

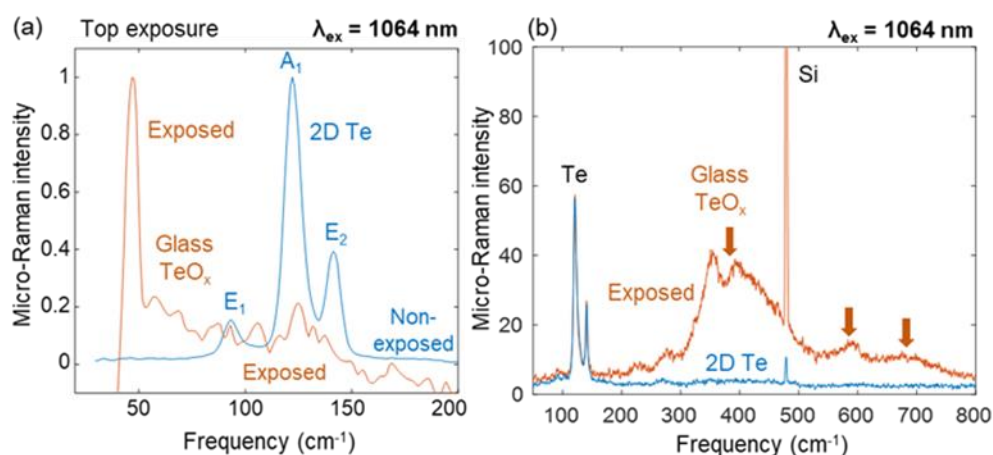


Figure S2. MicroRaman probed oxidation in 2D Te with 1064nm pulsed laser top excitations. a) On- (orange) and off- (blue) exposed spot. b) Broadband spectra exhibiting TeO_x peaks.

III. Top illumination processing with 532 nm cw laser

At increasing fluence (controlled by laser power with the same exposure time), the broadband background signal coming from glassy Te oxide rises with the laser power. An opposite trend is observed for the A_1 and E_1 peaks for 2D Te. Note that the in-situ micro-Raman spectra are collected during the high-power exposure (10% -100%), and the post-irradiation spectra are collected with 1% power to eliminate nonlinear material response.

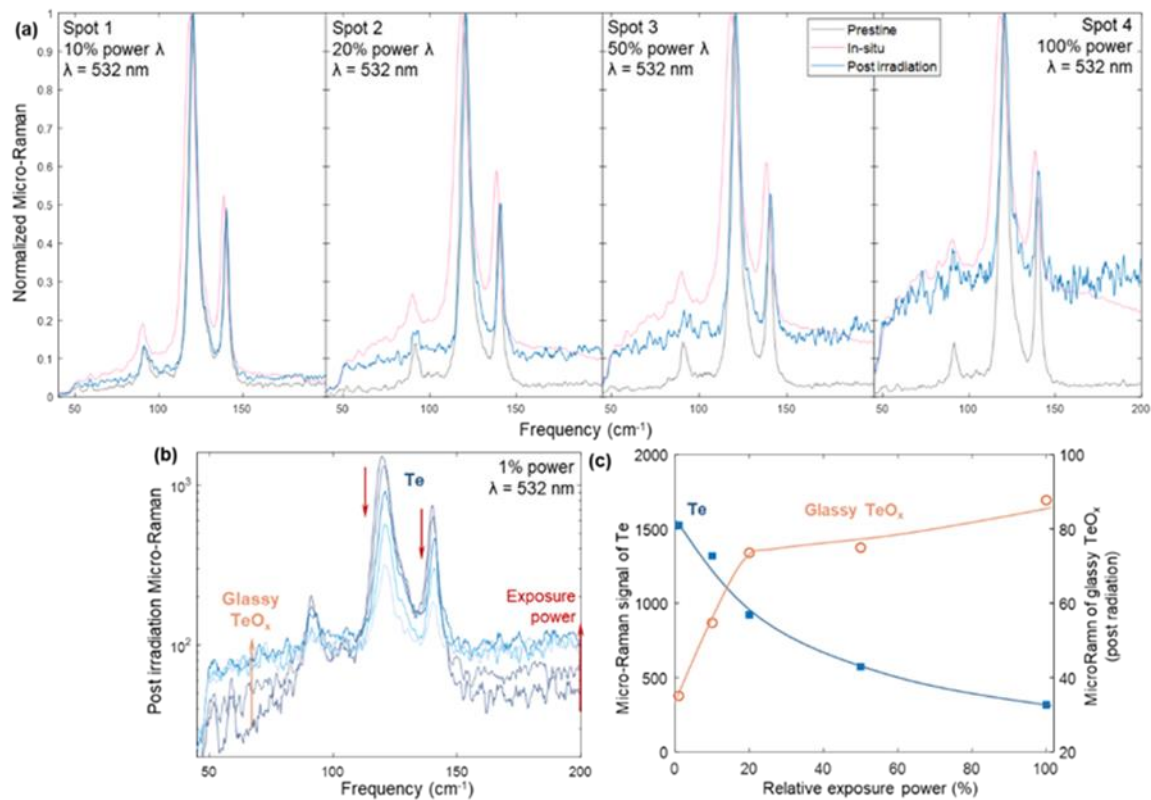


Figure S3. Micro-Raman probed oxidation in ~20 nm 2D Te with 532 nm c.w. laser top excitations. a) Normalized micro-Raman spectra of four different spots across flakes on the pristine sample (grey), in-situ monitoring at different exposure laser power (pink) and post-exposure (blue). b) Spectra of fluence-dependent post-exposure sample probed with low power. c) Micro-Raman signal level from Te oxide (~60 cm⁻¹ marked in b) with orange arrows and Te (A_1 peak) versus the laser power (labeled in a)).

IV. Schematics of 2D Te integration on silicon photonics

Firstly, we prepare the high-quality silicon photonic substrate manufactured in the foundry.^[S8] The top oxide is removed to expose the silicon microring resonator (MRR), and the rest of the supporting waveguide structures and couplers are protected under the thick oxide (Figure S4a-c). The solution-grown 2D Te are integrated into the arrays of high-quality MRRs (schematics, Figure S4d) through wet transferring (Figure S4ef) and dry transferring (Figure S4gh). To obtain high-quality 2D Te flake covered on the desired position of silicon devices, we utilize this dry transfer method.

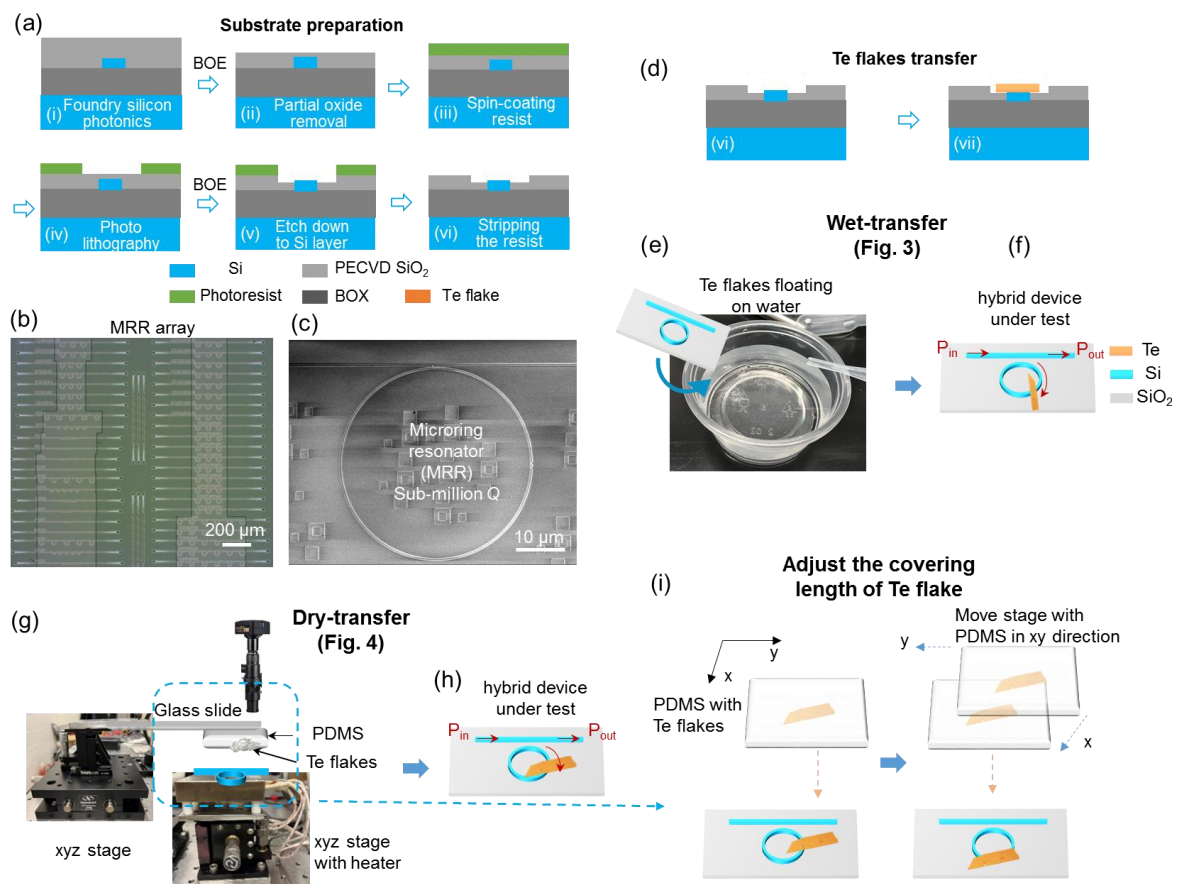


Figure S4. Schematics of device preparation. a) post-processing steps of the foundry-manufactured high-quality silicon MRRs. b) Optical microscope image of the open window after stripping the resist. c) Zoom-in SEM image of the exposed MRR to verify the exposure of the silicon device layer. d) Schematics of the Te flakes transfer process. e) Wet transfer and g) dry transfer process and correspondent devices (f, h). We only show two specific devices which results are fully analyzed in the main text. i) Schematics of adjusting the covering length of Te flakes in the dry transfer process.

Take one droplet of tellurium raw solutions to drop on one synthesized transparent PDMS on a glass slide. After solvent evaporation (~5 minutes), we flipped the glass with the PDMS side facing the SOI substrate and mount the glass slide on a separate xyz precision positioner (Figure S4g). The open-window silicon photonic sample is mounted on the other XYZ stage with a heating function. After aligning the desired 2D Te flake and the silicon MRR under the top camera, the glass slide landed on the silicon photonic substrate. Then we turn on the heating stage to bring the sample temperature to 70°C for 10 mins, to release the Te flake onto the target MRR. After releasing Te flakes, the PDMS-on-glass substrate is detached and removed (Figure S4h). For controlling the covering length of Te flakes over the silicon ring resonator, it can be done by moving the stage with PDMS in xy direction (Figure S4i). By carefully moving and aligning PDMS with the Te flake to the desired position on the silicon ring resonator with controllable covering length, it can be landed and released the Te flake on the silicon substrate.

V. Effective index extraction from the transmission spectra

By curve fitting the transmission spectra in Figure 3c and Figure 4c, the effective index change can be extracted after Te oxidized to glassy TeO₂. The transmission spectrum is shown as ^[S9]

$$T = \frac{|\gamma - \alpha * e^{-j\theta}|^2}{|1 - \alpha * \gamma * e^{-j\theta}|^2}, \quad (S1)$$

where γ is the transmission factor of a ring resonator, α is the linear loss of a ring, the phase $\theta = \frac{2\pi}{\lambda} n_{eff} L$, and L is the effective length.

By fitting the measured transmission spectra to the equation above, it is able to get the parameters of γ , α , and phase θ .

In this case of the hybrid device, the phase is contributed both from the Si waveguide without Te covering and Te covered Si waveguide: ^[S9]

$$\theta = \frac{2\pi}{\lambda} n_{eff_Si} L + \frac{2\pi}{\lambda} n_{eff_Te-Si} L_{Te}, \quad (S2)$$

where L_{Te} is the covering length of the Te flake (L_{Te} can be estimated from the optical image of the hybrid device), L is the perimeter of the Si ring ($L=2\pi R$, $R=20 \mu\text{m}$), n_{eff_Si} is the effective index of Silicon waveguide, n_{eff_Te-Si} is the effective index of Te covered Si waveguide.

After Te is oxidized to glassy-TeO₂, the phase difference ($\Delta\theta$) is only attributed to the effective index change due to oxidation:

$$\theta + \Delta\theta = \frac{2\pi}{\lambda} n_{eff_Si} L + \frac{2\pi}{\lambda} (n_{eff_Te-Si} + \Delta n_{eff_Te-TeO_2}) L_{Te}, \quad (S3)$$

where $\Delta n_{eff_Te-TeO_2}$ is the effective index change (corresponding to the values in Figure 3d, Figure 4d) due to Te oxidized to glassy TeO₂. The extraction of effective index change ($\Delta n_{eff_Te-TeO_2}$) due to oxidation has considered the effect of Te flake length (L_{Te}) from the equations above.

VI. 2D Te covering length-dependent intrinsic loss in silicon microring resonator

Other two hybrid Te-silicon devices have also been characterized to see how the intrinsic Q factor changes after being transferred with one Te flake. The hybrid device in Figure S5a has a thickness of 20 nm and a covering length of 1.3 μm . The intrinsic Q factor dropped a little from 152.2k to 151.9k (Figure S5b). Another hybrid device in Figure S4c has a thickness of over 30 nm and a covering length of 31 μm . The intrinsic quality factor dropped from 29.8k to 13.9k (Figure S5d).

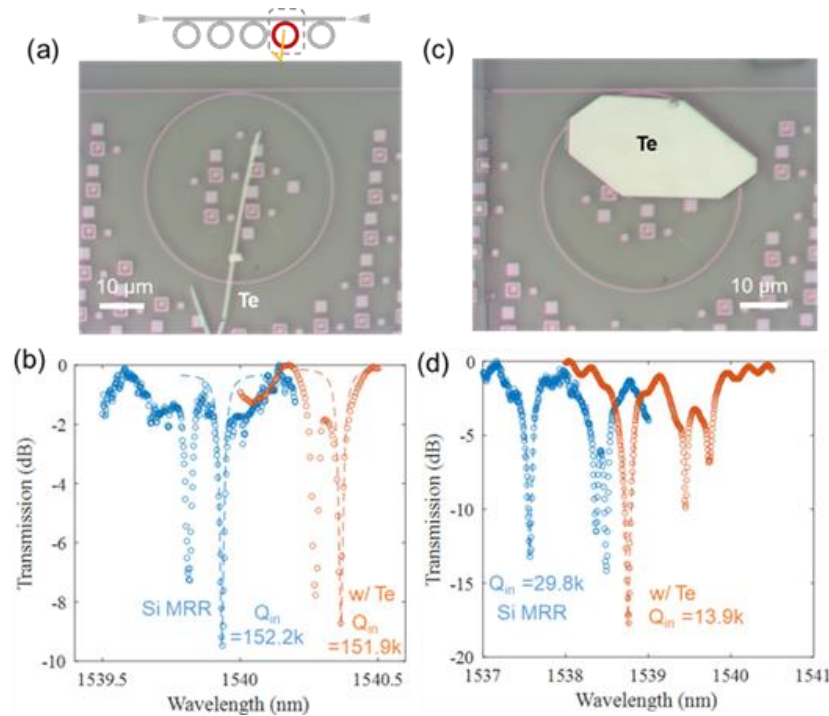


Figure S5. Exemplary devices showing the Te covering length-dependent intrinsic loss in silicon microring resonator (MRR). a) The optical microscope image of an MRR covered with $\sim 2\mu\text{m}$ covering the length of transferred Te flake. b) Corresponding transmission spectra in the MRR before transferring (with top oxide removed) (blue) and the same device after transferring (red). The resonance shift is attributed to the environmental temperature fluctuation over days. c) Another device with a much longer covering length (31 μm). d) Transmission spectra of the device in c before (blue) and after (red) transferring the Te flake.

References

- [1] C. Ríos, M. Stegmaier, P. Hosseini, D. Wang, T. Scherer, C.D. Wright, H. Bhaskaran, W. Pernice, *Nat. Photon.* **2015**, 9, 11
- [2] C. Wu, H. Yu, H. Li, X. Zhang, I. Takeuchi, M. Li, *ACS Photonics* **2018**, 6, 1

- [3] Y. Zhang, J.B. Chou, J. Li, H. Li, Q. Du, A. Yadav, S. Zhou, M.Y. Shalaginov, Z. Fang, H. Zhong, C. Roberts, P. Robinson, B. Bohlin, C/ Ríos, H. Lin, M. Kang, T. Gu, J. Warner, V. Liberman, K. Richardson, J. Hu, *Nature communications* **2019**, *10*, 1
- [4] T. Li, Y. Wang, W. Li, D. Mao, C.J. Benmore, I. Evangelista, H. Xing, Q. Li, F. Wang, G. Sivaraman, A. Janotti, S. Law, T. Gu, *Adv. Mater.* **2022**, *6*, 2108261
- [5] C. Castellan, A. Chalyan, M. Mancinelli, P. Guilleme, M. Borghi, F. Bosia, N.M. Pugno, M. Bernard, M. Ghulinyan, G. Pucker, L. Pavesi, *Opt. Express* **2018**, *26*, 4
- [6] Q. Xu, S. Manipatruni, B. Schmidt, J. Shakya, M. Lipson, *Opt. Express* **2007**, *15*, 2
- [7] D. Mao, M. Chen, X. Ma, A. Soman, H. Xing, T. Kananen, N. Augenbraun, C. Cheng, M. Doty, T. Gu, *Opt. Mater. Express* **2020**, *10*, 9
- [8] F. Wang, L. Zhao, Y. Xiao, T. Li, Y. Wang, A. Soman, H. Lee, T. Kananen, X. Hu, B. P. Rand, T. Gu, *Adv. Opt. Mater.* **2021**, *12*, 2100783
- [9] I. Datta, S. Chae, G. Bhatt, M. Tadayon, B. Li, Y. Yu, C. Park, J. Park, L. Cao, D. Basov, J. Hone, M. Lipson, *Nat. Photon.* **2020**, *14*, 256–262